NANO · MICRO small
www.small-journal.com

Bidirectional Voltage Regulation for Integrated Photovoltachromic Device Based on P3HT-Electrochromic Unit and Perovskite/Organic Tandem Solar Cells

*Yiming Bai, Shilei Tian, Yuzhe Guan, Xi Wang, Fuzhi Wang, Meicheng Li, Zhan'ao Tan, and Guicheng Liu**

Integrated electrochromic devices powered by photovoltaic cells have evoked a lot of interest due to their promising commercial prospects. However, their application has been restricted by the voltage adaption between the self-powered voltage and the color-changing threshold voltage (V_t). Herein, a strategy of bidirectional voltage regulating is proposed to develop a novel stand-alone integrated photovoltachromic device (I-PVCD), which integrates perovskite/organic tandem solar cells (P/O-TSCs) to drive color-changing process of conjugated poly(3-hexylthiophene) (P3HT) films. To lower the driving-voltage of electrochromic layer, C_{60} is introduced to decrease the onset oxidation potential of P3HT film, and thus leading to a reduced V_t of 0.70 V benefiting from the enhanced highest occupied molecular orbital level and decreased charge transfer resistance from 67.46 to 49.89 Ω. Simultaneously, PBDB-T is utilized as the hole transport layer in the interconnecting layer of $CsPbI_2Br$/PTB7-Th:IEICO-4F P/O-TSC to improve its open-circuit voltage (V_{oc}) to 1.85 V. Under their synergetic merits, a I-PVCD with a wider self-adaptive voltage range is achieved. This device can undergo fast and reversible chromic transition from beautiful magenta to transparent only under the solar radiation, and demonstrates a coloration efficiency of 351.90 cm^2 C^{-1} and a switching time of 2 s besides its excellent operating reliability.

1. Introduction

Increased energy consumption in modern construction industries has caused serious environmental pollution and energy shortage. Lots of studies show that the building energy consumption accounts for about 41% of the total energy utilization, and among the building energy consumption, lighting and air conditioning occupy more than 75%, which is closely related to door and window glass.[1,2] Electrochromic (EC) window can timely adjust its color and transmittance via detecting input signals and thus offsetting building energy needs by up to 40% as well as its beautiful colors integrating the human being's pursuit of poetical dwelling.[3–5] Nevertheless, the requirement for an external electrical supply causes the response-lag in optical modulation of electrochromic devices (ECDs) and restricts their application.[6]

To overcome this restriction, efforts have been directed to photovoltaic-driven electrochromic devices, which uses photovoltaic component supplies power to drive color-changing and then solves the optical modulation response-lag problem of ECDs. Generally, photovoltaic-driven electrochromic devices are classified into two categories of a four-terminal [7] and a two-terminal device architecture.[8] The former combines photovoltaic and EC units in a separated architecture, which is easy for fabrication but still suffers from necessitating external wiring and complicating installation.[9] Relatively, the later integrates

Y. Bai, S. Tian, Y. Guan, X. Wang, F. Wang, M. Li, Z. Tan, G. Liu
State Key Laboratory of Alternate Electrical Power System with Renewable Energy Sources
North China Electric Power University
Beijing 102206, China
E-mail: gcliu@ncepu.edu.cn
Y. Bai
Key Laboratory of Semiconductor Materials Science
Beijing Key Laboratory of Low Dimensional Semiconductor Materials and Devices
Institute of Semiconductors
Chinese Academy of Sciences
Beijing 100083, China
The ORCID identification number(s) for the author(s) of this article can be found under https://doi.org/10.1002/smll.202402903
G. Liu
School of Energy Power and Mechanical Engineering
North China Electric Power University
Beijing 102206, China
G. Liu
Beijing Laboratory of New Energy Storage Technology
North China Electric Power University
Beijing 102206, China

DOI: 10.1002/smll.202402903

photovoltaic and EC units in an all-in-one architecture, i.e., integrated photovoltachromic device (I-PVCD), and eliminates the cumbersome external wiring,[8] but still troubles by process compatibility. No matter what kind of device structure, PVCD can timely adjust the glass color and transmittance while realizing the photoelectric conversion, which presents a promising prospect in modern energy self-sufficient and aesthetically more appealing buildings.

Recently, there has been continuing interest in the emerging field of PVCD stimulated by the significant application value. Aubrey L. Dyer et al. demonstrated a vertically I-PVCD with a switching time of 3–6 s, and it could be reversibly switched between transparent and colored states via selectively connecting two of four electrodes of the PVCD device.[10] Alessandro Cannavale et al. combined a perovskite-based I-PVCD, which can realize a colorization from neutral-color semi-transparent to dark blue tinted together with a significant switch of average visible transmittance (AVT) from 26% to 16% and a power conversion efficiency (PCE) from 3.7% to 5.5% under illumination.[11] You Liu et al. reported an I-PVCD combining perovskite photovoltaic and ion-gel-based electrochromic components, and the pristine transmittance and contrast ratio of this I-PVCD reach up to 76% and 30%, respectively, on average visible transmittance (400–780 nm).[8] These studies confirm the potential and broad prospects of PVCDs. However, current studies meanly focus on a single ECD or a single photovoltaic device, and their all-in-one integration remains challenging. Even for single ECD, operating at high voltage would increase the energy consumption and result in a rapid device degradation.[12] But an extremely low-driving voltage (<1.0 V) has been still rarely reported, which is the most crucial issue to be solved for ECDs.[13,14] For PVCDs, in-depth studies are still scare due to two issues. The first relates to the matching issue between the solar cell's open-circuit voltage (V_{oc}) and the color-changing threshold voltage (V_t) of ECD. Namely, the outputting voltage of photovoltaic cell should be high enough to drive color-changing process of ECD. The second involves issues of process compatibility and electrochromic mechanisms. Hence, the objective of the present study is to perform the bidirectional voltage regulation of I-PVCDs, and address the aforementioned problems warranting fully exploration.

The poly(3-hexylthiophene) (P3HT) with unique electronic and optical properties has been extensively used in photovoltaics and effect transistors field,[15,16] but few studies focus on its application in electrochromic fields as its electrochromic mechanism is still not being fully understood and developing a low-driving voltage ECD is still unsolved.[17] Herein, an exploration toward reducing the driving-voltage of P3HT-based ECD and integrating it with perovskite/organic tandem solar cells (P/O-TSCs) is first conducted. To achieve I-PVCD with a broader adaptive-voltage range, C_{60} is introduced to reduce V_t of ECDs, and the results show a reduced V_t from 0.80 to 0.70 V besides a coloration efficiency (CE) from 280.37 to 351.90 $cm^2\ C^{-1}$ are achieved. Further electrochromic mechanism revealing these optimizations attribute to the enhanced highest occupied molecular orbital (HOMO) level and decreased charge transfer resistance from 67.46 to 49.89 Ω upon introduction of C_{60}. The ECD performance shows quantifiable improvement, and **Figure 1a** and Table S1 (Supporting Information) compares our work with the summary of state-of-the-art ECDs.[18–25] Furthermore, PBDB-T/MoO_3/Ag/PFN-Br is adopted as the interconnecting layer (ICL) of $CsPbI_2Br$/PTB7-Th:IEICO-4F perovskite/organic tandem solar cell (P/O-TSC), and its V_{oc} reaches up to 1.85 V benefitting from the obviously reduced interfacial trap density. Notably, the all-in-one I-PVCDs possess an excellent wide self-adaptable voltage range, operating reliability and swift transmittance adjustment with variable surrounding light intensity in real-time. Our findings pave the pathway for practical applications of this PVCD-based smart window.

2. Results and Discussion

2.1. Characterization of P3HT Electrochromic Film

To obtain ECDs with low driving-voltage, evaluating the onset oxidation potentials (*E*ox onset) is crucial since it is an important parameter that reflects the difficulty of oxidizing, reveals the reaction mechanism, and optimizes the electrochemical process.[26] Here, the influence of P3HT films' thickness on values of *E*ox onset is investigated. Figure S1a–c (Supporting Information) presents the corresponding cyclic voltammograms of PH3T films in the three-electrode system at a scan rate of 50 mV s^{-1}. The *E*ox onset increases from 0.355 to 0.404 V as the thickness of P3HT film is increased from 23 to 69 nm, as compared in Figure 1b. Generally, a higher *E*ox onset has several impacts on electrochromic materials (ECMs). The first involves a higher driving-voltage to undergo oxidation, resulting in slower color change kinetics in ECMs and thus prolonging the switching time.[27] Second deals with long-term durability because materials with higher oxidation potentials may be more susceptible to degradation or breakdown.[28] Last relates to CE since more energy is required to achieve a desired color change according to the definition of CE as Equation 1

$$CE = \frac{\Delta OD}{Q_d} = \frac{\log\left(\frac{T_b}{T_c}\right)}{Q_d} \quad (1)$$

where, ΔOD is the change in optical density (between bleached- and colored-state) at a given wavelength, Q_d is the necessary injected/ejected charge per unit area to induce a full switch, T_b and T_c are the transmittance in the bleached- or colored-state at a specific wavelength.[29] Obviously, the values of *E*ox onset decrease with increasing the thickness of P3HT film, and 23-nm P3HT film with a smallest *E*ox onset (0.355 V) predicts the lowest-driving-voltage and the highest CE. Figure 1b also manifests CE values of 23-, 45-, and 69-nm P3HT films, and they are 280.37, 208.02, and 184.75 $cm^2\ C^{-1}$, respectively. 23-nm P3HT film with the championed CE value indicates its ability of completely using injected charges, which is in good accordance with our prediction.

The cyclic voltammograms of 23-nm P3HT film after 1, 10, and 50 cycle(s) in 0.1 mol L^{-1} LiTFSI/anhydrous acetonitrile are further tested to assess its cyclability, as compared in Figure 1c. Clearly, three curves are almost overlapped, highlighting its outstanding cyclability and stability. Figure 1d–f presents the transmittance spectra and photographs of flowers seen through P3HT films with different thicknesses. As can be seen, all three samples (unbiased-state) exhibit deep transmission valleys (absorption peak) at 550 nm originated from the localized π–π^*

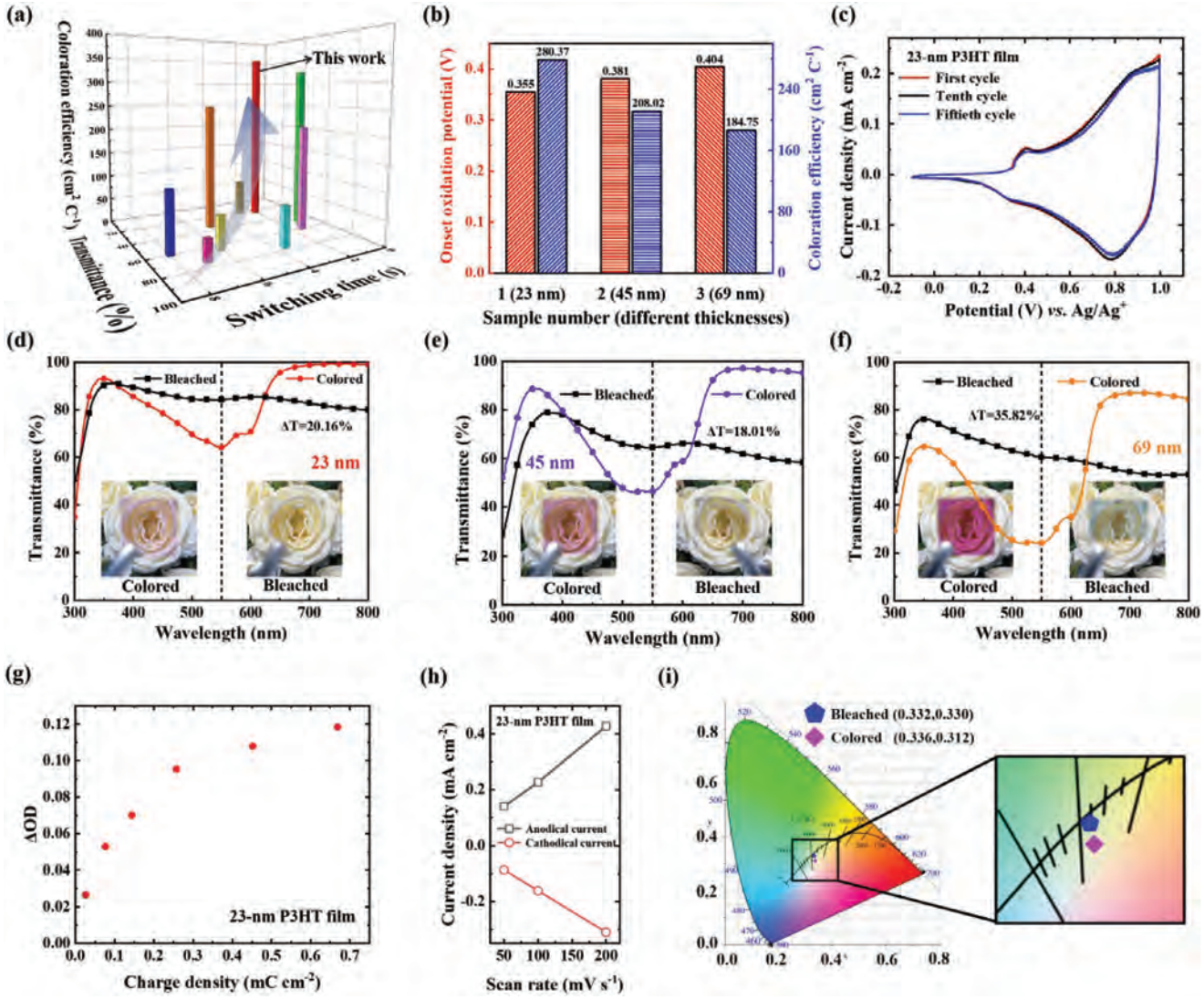

Figure 1. a) An overview of the state-of-the-art ECDs. b) Comparative analysis of the onset oxidation potential and coloration efficiency of P3HT films with varying thicknesses (23, 45, and 69 nm). c) Cyclic voltammograms of P3HT films after 1/10/50 cycle(s) [versus Ag/Ag^+] in 0.1 mol L^{-1} LiTFSI /anhydrous acetonitrile at a scan rate of 100 mV s^{-1}. Photographs of flowers viewed through d) 23-nm, e) 45-nm, f) 69-nm P3HT films and their corresponding transmittance spectra in the colored- (red) and bleached-state (black). g) Optical density as a function of charge density. h) Relationship between the peak current density and the scan rate. i) Color coordinates of 23-nm P3HT film in the colored- and bleached-state.

transitions,[30] implying the absorption of green light and the penetration of blue and red light result in the glass appearing magenta. The color gradually changes from light magenta to deep magenta with increasing film thickness, corresponding to the intensity of transmittance valleys gradually increases. When applied a 1.0 V bias (black curve), the transmittance valley vanishes within the visible region and high transmittance on the near-infrared region decreases strikingly, leading to almost flat transmittance spectra and the films appear translucent state from beautiful magenta.

Optical modulation is a key parameter to evaluate ECDs' potential application, which is defined as the maximum transmittance difference at a given wavelength ($\Delta T = T_b - T_c$). The ΔT at 550 nm are 20.16% (23 nm), 18.01% (45 nm) and 35.82% (69 nm) for P3HT films, respectively. Figure S1d (Supporting Information) displays the photonic response spectrum of human eyes, and the AVT and color rendering index (CRI) relied on the onset wavelength. Explicitly, the transmittance change at 550 nm locates at the most sensitive spectral range of human eyes, which is easy for eyes to perceive even with a slight color change, and therefore broadening their potential application field.

Based on the above analysis, 23-nm P3HT film is selected to measure its properties and further verify its potential application in I-PVCD. Plotting optical densities as a function of injected charge density results in a logarithmic correlation as shown in Figure 1g, which is not consistent with some ECMs with a linear correlation, indicating P3HT requires a small number of charges to drive a large transmittance change,[31] where the horizontal coordinate represents the amount of charge injected per unit area in the cyclic voltammetry and the vertical coordinate reflects the

Table 1. Experimental parameters of P3HT films with various thicknesses.

Thickness [nm]	T_b [%]	T_c [%]	ΔT [%]	ΔOD	Charge density [mC cm^{-2}]	CE [cm^2 C^{-1}]	AVT [B/C, %][a)]	CRI [B/C]
23	84.22	64.06	20.16	0.12	0.428	280.37	84.70/67.06	98.63/87.99
45	64.54	46.53	18.01	0.14	0.673	208.02	65.45/54.12	64.69/72.35
69	60.16	24.34	35.82	0.39	2.111	184.75	60.31/32.07	92.65/46.49

[a)] B/C in parentheses stands for bleached-or colored-state.

change of the optical density. As can be analyzed in Figure 1h, the peak current density increases linearly with the scan rate, suggesting a good adhesion between the electrochromic films and the ITO electrodes as well as the electrochemical process is facile and controllable.[17]

The CIE 1931 xyz chromaticity diagram is designed for human eye perception and can be used to evaluate the color characteristics of samples. Figure 1i illustrates the chromaticity diagram and color coordinates of P3HT films in the colored and bleached-states. The color coordinate of P3HT film in the colored-state is (0.336,0.312), which locates at the magenta region on the chromaticity diagram and emerges a beautiful magenta translucent glazing. For the bleached-state, the color coordinate is (0.332,0.330) with a CRI of 98.63 and an AVT of 84.70%, demonstrating super high color-neutrality and indicating objects seen through the P3HT film can commendably retain its original color based on the international standard—ISO 9050 glass in building.[32] The experimental parameters of P3HT films with different thicknesses are summarized in **Table 1**. The results obtained here allow the conclusion that 23-nm P3HT film is a desired candidate for I-PVCD.

2.2. Strategy of Reducing Color-Changing Threshold Voltage of P3HT Film

C_{60} with virtues of remarkable anti-corrosion and charge storage ability derived from its nanostructure of carbon in the Buckyball allotrope is expected to further reduce the *E*ox onset of P3HT film, and thus decreasing V_t and facilitating an easy self-driving electrochromic process. Lower *E*ox onset means that the electrochromic reactions are proceeded easily,[33] and the corresponding *E*ox onset of C_{60}/P3HT (0.315 V) and P3HT (0.355 V) are compared in cyclic voltammograms of **Figure 2**a,b. Therefore, it is reasonable to infer that an obvious decrease of V_t will be obtained based on the 40 mV change of *E*ox onset upon introduction of C_{60} film.

Switching time is one of important parameters to evaluate the features of ECDs, which is defined as the time required for the current density change by 90% between two constant voltages.[34] Figure 2c shows the curves of current density versus time at +1.0 and −1.0 V (versus Ag/Ag$^+$/ACN). C_{60}/P3HT film has a coloration process that takes about 2 s, which is less than that of P3HT (6 s). Similarly, the bleaching process of C_{60}/P3HT takes about 2 s, significantly lowering than that of P3HT (5 s) of P3HT. As the transmittance results in Figure 2d show, the transmittance of P3HT and C_{60}/P3HT at 550 nm for the colored-state are 64.06% and 62.96%, and 84.22% and 86.66% in the bleached-state, respectively. Consequently, the ΔT of P3HT and C_{60}/P3HT films are 20.17% and 23.70%. The charge densities of realizing color change for P3HT and C_{60}/P3HT films are 0.428 and 0.395 mC cm^{-2}, respectively, which indicate that C_{60}/P3HT requires a smaller number of charges to change color stemmed from its lower oxidation potential and higher HOMO. Consequently, a significant CE enhancement is achieved from 280.37 (P3HT) to 351.90 cm^2 C^{-1} (C_{60}/P3HT). The electrochromic parameters without and with C_{60} are listed in Table S2 (Supporting Information).

HOMO values of polymers are commonly used to assess the onset potential of oxidation process.[35] To elucidate the positive effects of C_{60}, the absorption spectra, the UPS and cyclic voltammetry were carried out to identify their HOMO levels, as shown in (Figure 2e–g). Tauc plots of P3HT and C_{60}/P3HT films calculated from UV–vis absorption spectra are shown in Figure 2e, and their bandgaps are 1.93 and 1.94 eV, respectively. Energy level parameters were calculated based on Figure 2f. The work function is obtained by calculating the difference between the incident light energy (He I, 21.22 eV) and the energy of the cut-off (P3HT:16.40 eV; C_{60}/P3HT: 16.67 eV), and the HOMO level is the sum of the onset (P3HT: 0.44 eV; C_{60}/P3HT: 0.47 eV) and the work function (P3HT: 4.82 eV; C_{60}/P3HT: 4.55 eV). The lowest unoccupied molecular orbital (LUMO) level is the difference between the HOMO (P3HT: −5.26 eV; C_{60}/P3HT: −5.02 eV) and work function.[36] Hence, the LUMO levels of P3HT and C_{60}/P3HT films are −3.33 and −3.08 eV, respectively.

The cyclic voltammetry (Figure 2g) is measured to explore the energy level change. the HOMO and LUMO levels of P3HT (−5.00 eV, −3.48 eV) and C_{60}/P3HT (−4.78 eV, −3.49 eV) are calculated according to $E_{HOMO/LUMO} = -e(\varphi_{ox}\text{“}/\varphi_{red}\text{”} +4.36)$, respectively. Although there is a slight difference between results from UPS and Cyclic voltammetry, but the changing trend is in good accordance and the influence is mainly on the enhancement of HOMO level. P3HT is served as the donor unit and C_{60} is played as the acceptor role in C_{60}/P3HT film, and the strong interaction between the donor and acceptor units will boost the HOMO energy levels of polymers, leading to the decrease of *E*ox onset.[37,38] A reasonable postulation could be concluded that the introduction of C_{60} may change the electron density of donor unit in P3HT chain and enhance the interaction with thiophene groups. Correspondingly, the boosted interaction between C_{60} and P3HT predicts more efficient charge transfer, which means an easier electron excitation at applied voltages and a decrease of color-changing voltage.

The improvement of electrochromic performance was further certified via Nyquist diagrams, as exhibited in Figure 2i, and the inset presents the equivalent circuit model. In the circuit, R_s is the series resistance, representing the contribution of electrolyte.

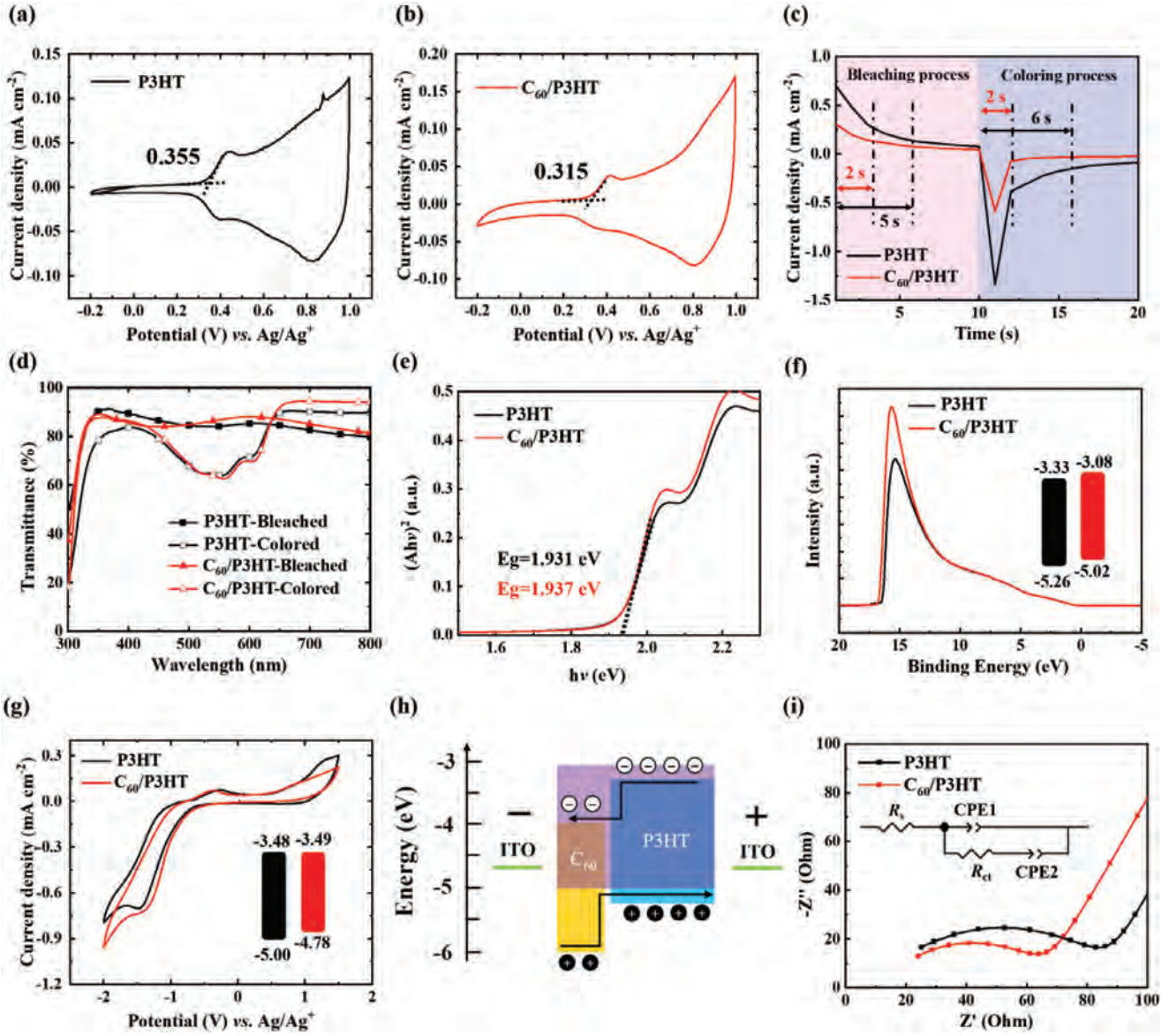

Figure 2. Cyclic voltammograms of a) P3HT and b) C_{60}/P3HT [versus Ag/Ag^+] recorded in 0.1 mol L^{-1} LiTFSI /anhydrous acetonitrile at a scan rate of 50 mV s^{-1}. c) Current densities versus time switching between 1.0 V (colored-state, 10 s) and −1.0 V (bleached-state, 10 s). d) Transmittance spectra of P3HT and C_{60}/P3HT in the colored- and bleached-state. e) Tauc plots of P3HT and C_{60}/P3HT films calculated from the UV–vis absorption spectra. f) UPS spectra of P3HT and C_{60}/P3HT films. g) The cyclic voltammetry curves of P3HT and C_{60}/P3HT in 0.1 mol L^{-1} $[nBu_4N]^+[PF_6]^-$/ACN using a scan rate of 20 mV s^{-1}. i) Nyquist diagram of P3HT and C_{60}/P3HT films at an DC potential of 0.4 V, and the inset is the equivalent circuit model.

R_{ct} is the charge-transfer resistance, accounting for the interfacial faradaic process. The constant-phase element CPE1 denotes the double-layer capacitance between the polymer film and electrolyte, and CPE2 reflects the low-frequency capacitance associated with film charge storage. The non-ideality factor n_{CPE} associated with the constant-phase element ranges from 0 to 1, indicating resistance when n = 0 and capacitance when n = 1. Ideally, the constant-phase element represents a capacitor when n = 1. The fitting results are compared in **Table 2**.

As the results in Table 2 demonstrate, the values of R_s and R_{ct} for P3HT are 16.80 and 67.46 Ω, respectively. While for C_{60}/P3HT, they are 13.66 and 49.89 Ω, respectively. The decrease in the R_{ct} values of C_{60}/P3HT clearly suggests that the charge-transfer process at the polymer/electrolyte interface is being facilitated. The *E*ox onset depends on interactions between the electrode and electrolyte interface, which means that the electrochromic reactions of C_{60}/P3HT-based ECD are proceeded more easily, and switching time becomes shorter.[39,40] Meanwhile, the value drop of R_s points out that C_{60}/P3HT with a smaller oxidation–reduction potential will experience more complex electrochemical process than P3HT,[41] and thus influencing the parameters of electrolyte and leading to a lower R_s. CPE1 value relates to film morphology. The value of C_{60}/P3HT rises apparently than that of P3HT, indicating an expansion of

Table 2. Parameters obtained from the electrochemical impedance data fitting.

Type	R_s [Ω]	R_{ct} [Ω]	CPE1 [10^{-6} F]	n_{CPE1}	CPE2 [10^{-3} F]	n_{CPE2}
P3HT	16.80	67.46	1.26	0.77	0.32	0.66
C_{60}/P3HT	13.66	49.89	1.96	0.76	0.40	0.65

effective contact area in the polymer/electrolyte interface.[42,43] Both n_{CPE1} and n_{CPE2} retain almost the same value before and after introducing C_{60}, revealing the charge distribution in P3HT film is maintained at the same configuration.[40]

2.3. C_{60}/P3HT-Based ECD with Excellent Reversibility and Stability

C_{60}/P3HT with advantages of lower *E*ox onset, suitable energy level, faster switching time and reduced R_{ct} was used to fabricate ECDs. Instead of using the traditional liquid electrolyte, the gel electrolyte based on polyvinylpyrrolidone was used as the ion transport layer to solve possible leakages of liquid electrolyte. The structure and color switching mechanism of ECD are shown in **Figure 3**a, in which the device appears gorgeous magenta of the original P3HT in natural conditions (unbiased-state), and shows neutral-semitransparent color (biased-state) due to the P3HT oxidation under a forward bias. During the process, the reduction of C_{60} connected to positive terminal occurs and begins to accumulate electrons received from P3HT after oxidation, and simultaneously P3HT in oxidation generates transparent polarons (middle panel of Figure 3a). Corresponding to the switching from magenta to translucency. When applied a reversed bias potential, the polarons take electrons accumulated in C_{60} and make P3HT return to the neutral state again with a color response from translucency to magenta (right panel of Figure 3a). It is important

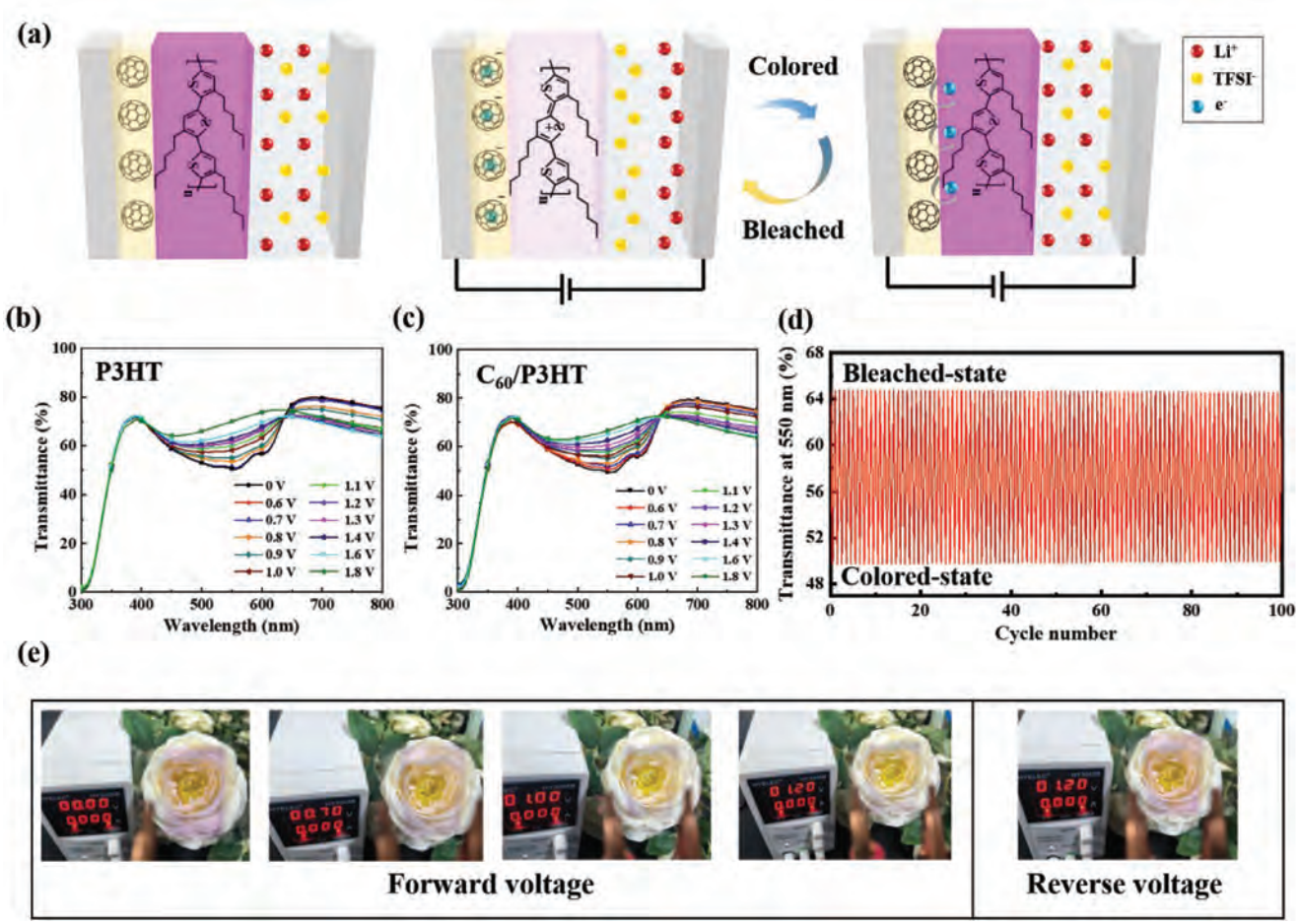

Figure 3. a) Schematic diagrams of device structures and working principles of C_{60}/P3HT-based ECD. Transmittance spectra of b) P3HT- c) C_{60}/P3HT-based ECDs by applying an external voltage bias (0–1.80 V). d) Periodic transmittance at 550 nm for C_{60}/P3HT-based unencapsulated ECD switching between colored-state (−1.60 V for 30 s) and bleached-state (1.60 V for 30 s). e) Digital images of flowers viewed through ECDs by applying different external voltage biases with the device responsive state from tinted, to bleached, then re-tinted again.

to emphasize that C_{60} plays an important role of reducing onset oxidation potential and facilitating polaron formation.

The electrolyte layer concluding LiTFSI and polyvinylpyrrolidone is used to stabilize polarons formed at positive bias voltage, in which $TFSI^-$ ions will get dissociated and be attracted to polarons, thus balancing the charge in the whole device. This electrochromic process is detailed in the following expression.[44]

$$\underset{\text{(neutral)}}{P3HT^0} + TFSI^- \underset{\text{reduction}(+e^-)}{\overset{\text{oxidation}(-e^-)}{\rightleftarrows}} \underset{\text{(polaron, radical cation)}}{P3HT^{+\bullet}TFSI^-} \quad (2)$$

Figure 3b,c presents the transmittance spectra of P3HT and C_{60}/P3HT films under different bias voltages (V_f). Evidently, the transmittance valleys (absorption peak) both for unbiased P3HT and C_{60}/P3HT locate at 550 nm (colored-state), and it gradually vanishes (bleached-state) as V_f increases until the transmittance spectra demonstrate a flat shape when the applied voltage is up to 1.80 V, which means the totally bleaching behavior occurring. On the whole, their bias-driven transmittance spectra demonstrate almost similar trend and appear more and more flatter shape in the visible range (370–760 nm) when V_f is higher than 1.20 V, indicating that ECDs can achieve good bleached-states if the driving-voltage is higher than 1.20 V. However, an obvious transmittance change of C_{60}/P3HT can be observed at $V_f = 0.70$ V in contrast to $V_f = 0$ V, which can be defined as V_t of ECD according to previous reports.[45–47] On the contrary, there is no obvious transmittance change for P3HT until $V_f = 0.80$ V, revealing the required threshold voltage of C_{60}/P3HT ($V_t = 0.70$ V) is lower than that of P3HT ($V_t = 0.80$ V).

According to the definition of V_t, the voltage corresponding to the abrupt surge of current density in the cyclic voltammograms is defined as the threshold voltage of color changing, and the current density remains close to zero up to V_t. Definitely, V_t is characterized by the onset of intercalation of ions into the host oxide, which are correlates with *E*ox onset of ECMs. In our experiments, samples deposited on indium tin oxide (ITO) glass, silver/silver chloride (Ag/AgCl) wire and platinum (Pt) wire were used as working electrode, reference electrode and counter electrode, respectively. In consideration of the potential of reference electrode (0.205 V, 25 °C), the V_t of P3HT (0.56 V) and C_{60}/P3HT (0.52 V) films can be deduced from Figure 2a,b, stating a visual color changing will take place at this bias. Nevertheless, the V_t of ECDs are higher than that of films in our experiments, we speculated maybe derived from threes issues. First, the ionic conductivity of electrolyte is higher than that of gel electrolyte. Second, the conductivity of Pt at room temperature (≈6.7×10^6 S m^{-1}) exceeds ITO (about 10^5–10^6 S m^{-1}). Third, the differences of interfacial contact resistance between functional layers, such as the electrode/EC layer and the electrolyte/EC layer et al. Further calculating results show that ΔT of C_{60}/P3HT rises from 2.26% ($V_f = 0.70$ V) to 16.82% ($V_f = 1.80$ V). Though the value of ΔT is not high, but it is easy to capture the color change because the wavelength is located at the most sensitive area of human eyes.

To assess the C_{60}/P3HT-based ECD reversibility and reliability, the periodic transmittance at 550 nm for C_{60}/P3HT-based ECD switching between colored-state (−1.60 V for 30 s) and bleached-state (1.60 V for 30 s) was measured. Delightfully, ΔT remains to be 14.59% from initial 15.06% after 100 cycles (Figure 3d), revealing excellent cycling stability of C_{60}/P3HT-based ECD. Figure 3e displays the photographs of colored-, bleached-, and recolored-state of ECD by applying different forward and reverse voltages. Clearly, bias-driven device automatically switches colored- and bleached-states, which exhibits obvious and fully bleaching behavior when applied a forward voltage of 0.70 V and 1.20 V, respectively. If a reverse potential bias of 1.20 V was applied, the device returns to the magenta state again. To summarize, ECD exhibits excellent reversibility and stability as well as low threshold voltage, making it appropriate for use as the EC component of all-in-one I-PVCDs.

2.4. Perovskite/Organic Tandem Solar Cells with High Voltage

The outputting voltage of photovoltaic unit should be high enough to drive the operation of ECD. Here, TSCs are set to supply driving-voltage of ECDs in consideration of outdoor light intensity adjustment in real-time and the timely voltage response of tandem solar cells. All-inorganic perovskite $CsPbI_2Br$ with merits of excellent photoelectric properties, high stability and low preparation cost was used as the front sub-cell, and the organic photoactive layer of PTB7-Th:IEICO-4F was served as the rear sub-cell, connecting by PBDB-T/MoO_3/Ag/PFN-Br interlayer to construct the monolithic P/O-TSCs. Simultaneously, to improve TSCs' working voltage and deeply understand the working mechanism of the inter layer, PTB7-Th/MoO_3/Ag/PFN-Br and P3HT/MoO_3/Ag/PFN-Br are also used in TSCs as the control device since the output voltage is strongly rely on ICLs. Particularly, 1-nm Ag layer is deposited to fully realize the recombination of photogenerated-electrons and -holes in the interlayer. **Figure 4a** shows the schematic architecture of P/O-TSC and its cross-section SEM image, in which the thicknesses of $CsPbI_2Br$ and PTB7-Th:IEICO-4F 360 and 220 nm, respectively.

Figure 4b displays the schematic energy level of materials involved in this work. It should be highlighted that PBDB-T, PTB7-Th and P3HT all demonstrate the graded heterojunctions with that of $CsPbI_2Br$ and SnO_2, favoring electrons collection and reducing the recombination loss between $CsPbI_2Br$ and PBDB-T (or PTB7-Th, P3HT). Figure 4c presents the molecular structures and the microscopic passivation mechanism of PBDB-T on the perovskite surface, respectively. Our previous researches have shown that the under-coordinated Pb^{2+} defects in $CsPbI_2Br$ films can be passivated because the S atoms of Lewis thiophene can form bonds with Pb atoms, and efficaciously promotes the delocalization of electronic distribution.[48] As the results in Figure 4c demonstrate, the PBDB-T possesses more active component of Lewis thiophene in contrast to PTB7-Th and P3HT, which is conductive to passivate perovskite film. Meanwhile, the thiophene side chains are favorable for boosting film quality with dominant "face-up" orientation and increasing the hole mobility for a smoother charge transport.[49,50]

A careful study on the photovoltaic performances of P/O-TSCs was conducted to evaluate the feasibility of PBDB-T. Figure 4d,e shows *J*–*V* curves and EQE of three P/O-TSCs with different HTLs (PBDB-T, PTB7-Th, and P3HT) in the ICL. The corresponding photovoltaic parameters are compared in **Table 3** (average over 12 devices). As expected, PBDB-T-based device exhibits the best photovoltaic performances, especially the V_{oc} of 1.853 V when compared with that of PTB7-Th- (1.839 V) and P3HT-based

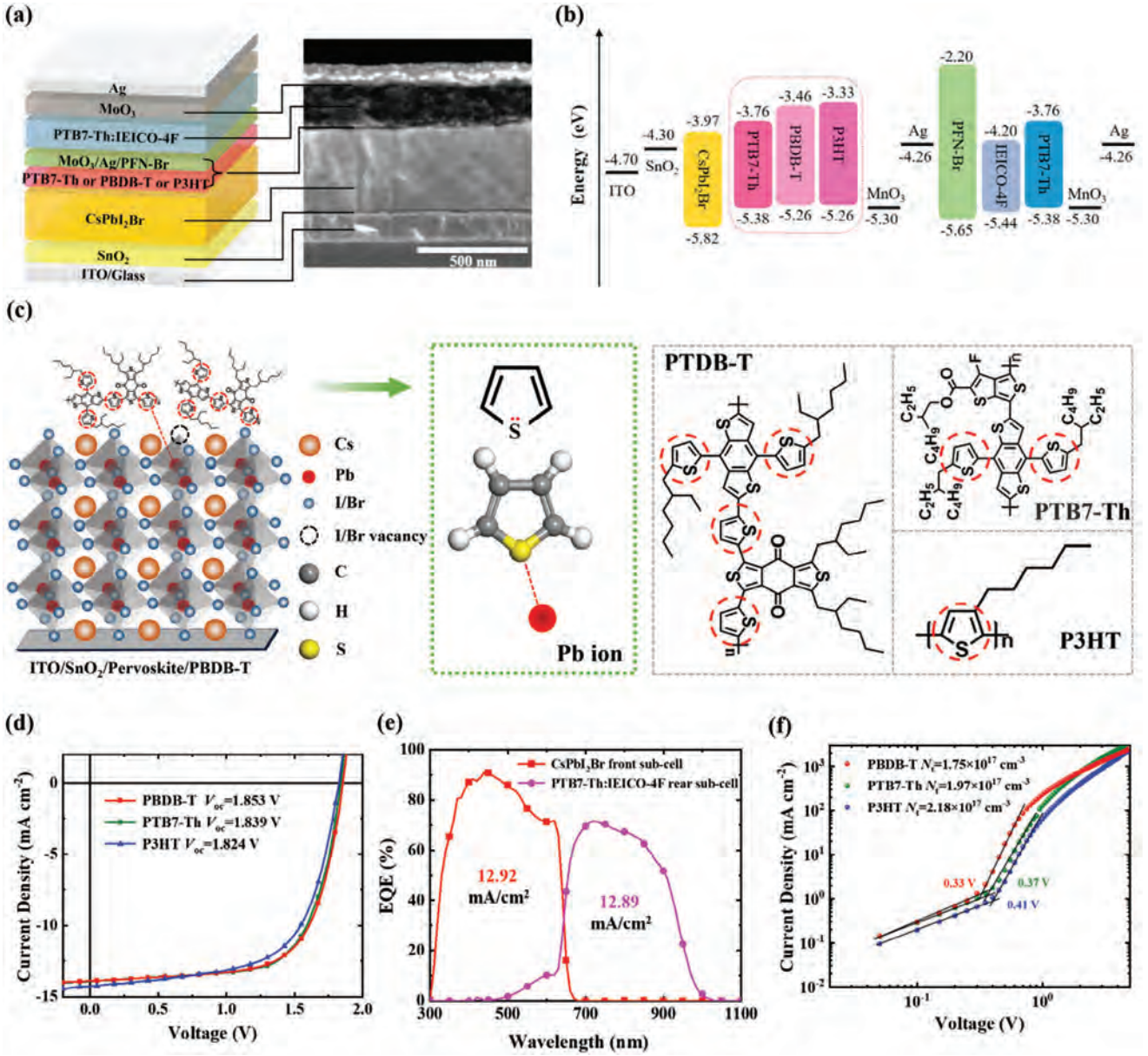

Figure 4. a) Schematic architecture of P/O-TSC and its cross-section SEM image. b) Schematic energy level and c) passivation mechanism and chemical structures of materials involved in this work. d) *J–V* curves and e) EQE spectra of monolith P/O-TSC with PBDB-T layer. f) Dark *J–V* characteristics of hole-only devices with different interconnection layers.

cells (1.824 V). Further analysis on device resistance finds a significant increase of shunt resistance (R_{sh}´) for PBDB-T-based P/O-TSCs (1540.83 Ω cm^2) than that of PTB7-Th- (1367.24 Ω cm^2) and P3HT-based devices (986.31Ω cm^2). Unsurprisingly, the lowest R_{sh}´of P3HT-based is obtained due to the weak passivation effects, and the cause for this is certainly derived from less active component of Lewis thiophene in its monomer structure. As a result, it is reasonable to speculate that the enhancement of V_{oc} is caused by the obvious decrease of interfacial leakage current due to the excellent passivation effects of PBDB-T, in which Lewis thiophene offers more S atoms to bond with undercoordinated Pb^{2+} defects. PBDB-T-based device displays a champion PCE of 18.15% with a short circuit current density (J_{sc}) of 13.89 mA cm^{-2}, and a fill factor (FF) of 70.52%. The PTB7-Th-based device obtains a PCE of 18.11% with a J_{sc} of 13.89 mA cm^{-2} and an FF of 70.86%. Figure S2 (Supporting Information) shows *J–V* curves of PBDB-T-based P/O-TSCs under the forward and reverse scanning modes with the corresponding photovoltaic parameters in Table S3 (Supporting Information), displaying a slightly hysteresis behavior.

Dark *J–V* characterization was carried out to verify the function of PBDB-T using the hole-only devices with an architecture of ITO/PEDOT:PSS/HTL/Au. The ohmic response within the low bias voltage results in a linear correlation as shown in Figure 4f. As the bias voltage is increased, the injected-current steeply increases at the intermediate region due to the space charge-limited

Table 3. Photovoltaic parameters for TSCs with different HTLs under illumination of AM 1.5G, 100 mW cm^{-2} (averaged over 12 individual devices).

HTL in the ICL	V_{oc} [V]	J_{sc} [mA cm^{-2}]	FF [%]	PCE [%]	R_s ′[Ω cm^2]	R_{sh} ′[Ω cm^2]
PBDB-T/MoO_3	1.853	13.89	70.52	18.15	13.19	1540.83
PTB7-Th/MoO_3	1.839	13.89	70.86	18.10	13.94	1367.24
P3HT/MoO_3	1.824	14.26	62.59	16.28	15.78	986.31

characteristics,[51] which is defined as the trap filling process. Consequently, the trap fill limit voltage (V_{TFL}) is quantified as the kink point between the two regions,[52] which is inversely proportional to the density of trap states (N_{trap}) according to Equation 2:

$$N_{trap} = \frac{2\epsilon_0 \epsilon V_{TFL}}{eL^2} \quad (3)$$

where e is the elementary charge, ϵ_0 and ϵ are the vacuum permittivity and relative dielectric constant (generally the value of ϵ is 3 for OSCs), and L is the thickness of the hole-only device. The V_{TFL} are 0.33, 0.37 and 0.41 V for PBDB-T-, PTB7-Th-, and P3HT-based devices, respectively. Correspondingly, the N_{trap} of PBDB-T, PTB7-Th, and P3HT are 1.75×10^{17}, 1.97×10^{17}, and 2.18×10^{17} cm^{-3}, respectively. The results confirm that PBDB-T has the lowest trap state density, lessening interfacial trap recombination and improving V_{oc}. From the results obtained up till now, we can confirm that PBDB-T/MoO_3/Ag/PFN-Br interlayer can effectively improve the operating voltage of P/O-TSCs.

2.5. Integrated Photovoltachromic Device with a Broader Adaptive Voltage Range

Aiming to develop I-PVCD with a broader adaptive voltage range between the driving-voltage of ECD and operating voltage of photovoltaic unit, we fabricated I-PVCDs via combining C_{60}/P3HT-based ECD and $CsPbI_2Br$/PTB7-Th:IEICO-4F P/O-TSC. **Figure** 5a shows the schematic architecture and working principles of the novel solar-adaptable I-PVCD. The bottom glass substrates with patterned ITO were both used as the common electrode (PV and ECD) and simultaneously avoid possible recombination current occurred around photovoltaic cells via etching electrode pattern. Photovoltaic and EC layers were fabricated sequentially (detailed process can be found in Experimental section). Low resistivity copper wire is used to connect the independent top electrodes, where ITO-coated top glass is the ECD electrode and Ag film is applied as the photovoltaic electrode. To drive color-fading, the I-PVCD is exposed to the natural surroundings, and photovoltaic cell generates adequate power to drive the operating of ECD. The photographs of I-PVCD prototype devices at colored- and bleached-state in natural surrounding are shown in Figure 5b. To further assess the optical performances of I-PVCDs, the transmittance spectra under different incident light intensities are characterized using UV–vis spectrometer (Figure 5c). As can be seen, the deep transmittance valley locate at the vicinity of 550 nm are also observed for unbiased-driven ECD component, which will disappear under natural condition under sunlight intensity from 0.3 to 1-sun. Both CRI and ΔT rises strikingly as the sunlight intensity increased besides AVT, and their all appears neutral color. I-PVCD under 1-sun illumination clearly exhibits an outstanding CRI of 93.63, an AVT of 70.71% and a ΔT(%) of 16.13% in contrast to that of unbiased-state (a CRI of 87.47 and an AVT of 57.05%). More parameters can be seen in **Table** 4. The results point out that the driving-voltage supplied by photovoltaic component under 0.3-sun is high enough to enable EC unit to change its color completely. Meanwhile, I-PVCD can adjust transmittance automatically in real time relying on the external solar intensity, which establish significant potentials for applications as modern all-day smart windows.

To further understand the difference between driving-voltage and V_{oc} of photovoltaic component, an in situ monitor is carried out to obtain the driving-voltage supplied by photovoltaic component under different sunlight intensities. Figure 5d,e plot I-PVCD's equivalent-circuit diagram and the experimental driving-voltage as a function of light intensity when I-PVCD is smoothly operating under natural sunlight. The results manifest that the driving voltage is almost equals to V_{oc}, confirming that the EC unit works as a capacitor with an extremely-low series resistance.

The switching reliability of unencapsulated I-PVCD were carried out as shown in Figure 5f, in which a slightly of ΔT decay can be viewed from 16.13% to 15.68% after 100 cycles constant working in air condition. The results obtained in this work allow the conclusion that our stand-alone I-PVCDs with broader self-adaptive voltage range, outstanding optical properties, switching stability and fast response time establish significant potentials for practical applications in modern energy-saving skyscrapers or smart display field.

3. Conclusion

In summary, a strategy of bidirectional voltage regulation is proposed here to achieved a stand-alone I-PVCD combining a P3HT-based EC unit and $CsPbI_2Br$/PTB7-Th:IEICO-4F-based photovoltaic cell. C_{60} with outstanding charge storage ability is introduced to reduce the onset oxidation potential (from 0.355 to 0.315 V) of P3HT-based ECD and therefore decreasing the color-changing threshold voltage from 0.80 to 0.70 V besides a CE enhancement from 280.37 to 351.90 cm^2 C^{-1}, a switching speed from 6 to 2 s and the optical modulation from 20.16% to 23.70% after incorporating C_{60}. Further electrochromic mechanism revealing these optimization attributes to the enhanced HOMO and a reduced charge transfer resistance after introducing C_{60}. PBDB-T is used to improve photovoltaic voltage and drive ECD unit work smoothly. A V_{oc} of 1.85 V is obtained due to the remarkable reduction of interfacial trap densities. Delightfully, the I-PVCD with excellent wide self-adaptable voltage range and excellent optical features is achieved. Further investigations on PVCD operating stability show that the optical modulation remains

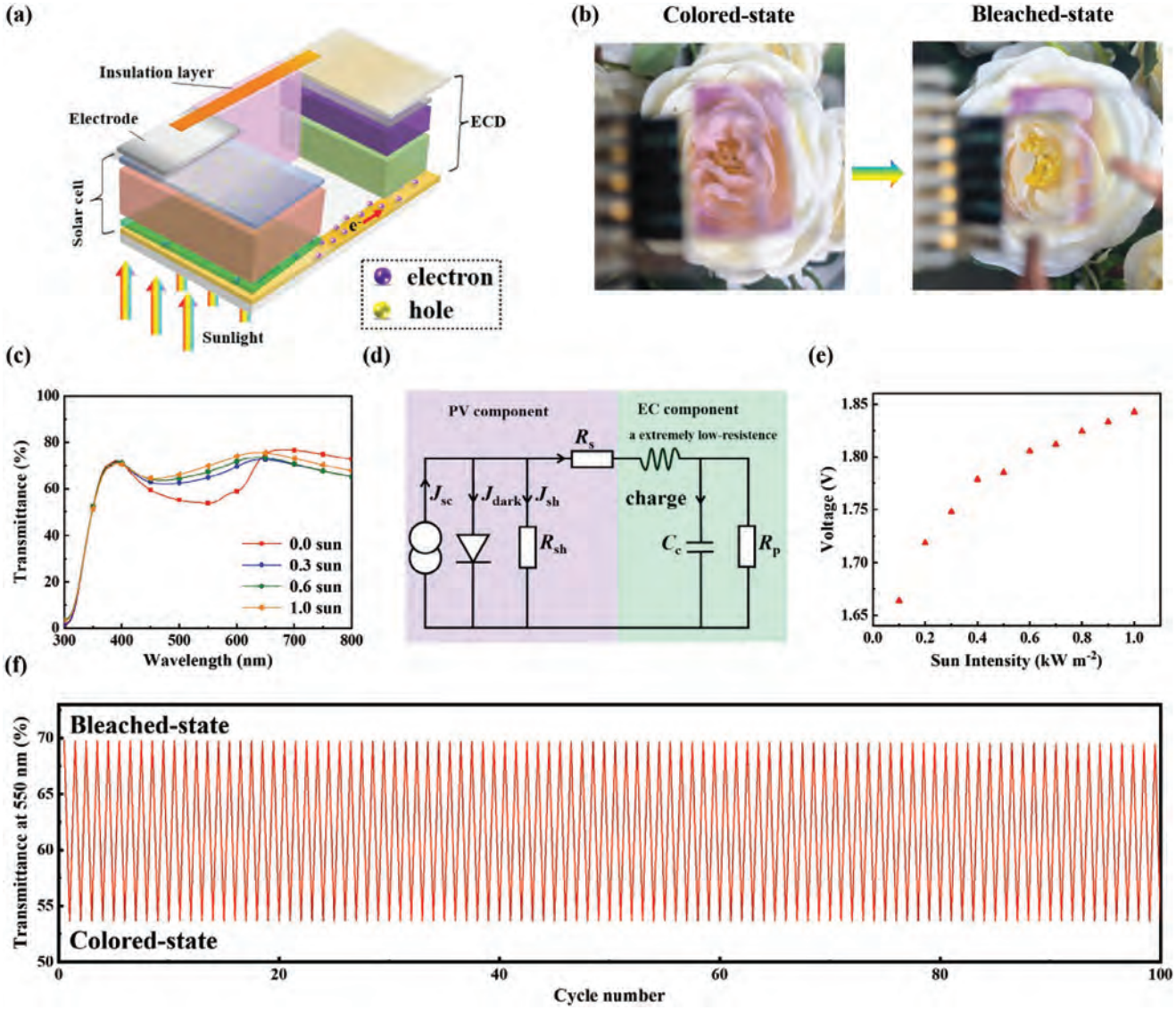

Figure 5. a) Schematic diagram of I-PVCD architecture and its working principles. b) Photographs of flowers observed through I-PVCD under colored- and bleached-state with a self-driven color-changing process. c) Real-time transmittance of I-PVCD illuminated by different sunlight intensities from 0.3 to 1.0 sun and at unbiased-state. d) Equivalent-circuit diagram of the I-PVCD. e) Driving-voltage versus of sunlight intensity. f) Periodic transmittance at 550 nm for unencapsulated I-PVCD switching between colored-state (without solar illumination) and bleached-state (under 1-sun illumination).

almost unchanged. These noteworthy results demonstrate that I-PVCDs with energy generation capability and aesthetic values have great potential applications in photovoltaic building integration and advanced electronic displays.

4. Experimental Section

Materials: Lithium bis((trifluoromethyl)sulfonyl)azanide (LiTFSI, 99%), cesium iodide (CsI, 99.999%), lead(II) iodide (PbI_2, 99.999%) and lead(II) bromide ($PbBr_2$, 99.999%) were purchased from Xi'an Yuri Solar Co., Ltd. (Xi'an, China). The organic materials of P3HT, PBDB-T, PTB7-Th, PFN-Br, IEICO-4F were purchased from Solarmer Material Inc. (Beijing, China). Chlorobenzene (99%), ethanol (99.5%), 1,2-dichlorobenzene (ODCB, 99%), acetonitrile, (ACN, 99.9%), C_{60}, polyvinylpyrrolidone and methanol (99.9%) were purchased from Innochem Technology Co., Ltd. (Beijing, China). Tin oxide (SnO_2) (15% in H_2O colloid dispersing solution), chloroform (CF), molybdenum trioxide (MoO_3), dimethyl sulfone (DMSO, 99%) and 1-chloralin were purchased from Alfa Aesar (Shanghai, China). All materials and solvents were used without further purification.

I-PVCD Fabrication: *Solution Preparation*: P3HT (10/20/30 mg mL^{-1}) was dissolved in ODCB and stirred for 12 h to obtain electrochromic material. polyvinylpyrrolidone (0.25 g) was dissolved in a electrolyte (1.0 mL, 0.1 mol L^{-1} LiTFSI/anhydrous ethanol)] to obtain gel polymer electrolyte. C_{60} (5 mg mL^{-1}) was dissolved in chlorobenzene and stirred for 6 h to obtain C_{60} solution. SnO_2 was dissolved in deionized water in a volume ratio of one to five and stirred for 2 h to obtain the solution. CsI (1.2 mol L^{-1}), PbI_2 (0.6 mol L^{-1}) and $PbBr_2$ (0.6 mol L^{-1}) were dissolved in DMSO and stirred at 60 °C for 2 h to obtain the $CsPbI_2Br$ precursor solution. P3HT (10 mg mL^{-1}), PBDB-T (10 mg mL^{-1}) and PTB7-Th (10 mg mL^{-1}) were dissolved in chlorobenzene and stirred for 6 h to obtain solutions, respectively. PFN-Br (0.5 mg mL^{-1}) was dissolved in

Table 4. Optical and electrical parameters of I-PVCDs under different sunlight illumination (averaged over 12 individual devices).

Sunlight intensity [kW m^{-2}]	Transmittance at 550 nm [%]	ΔT in 550 nm [%]	AVT [%]	CRI	Driving voltage [V]
1.0	69.80	16.13	70.71	93.63	1.843
0.6	67.36	13.69	68.51	94.74	1.806
0.3	64.83	11.16	66.31	93.82	1.748
0.0	53.67	–	57.05	87.47	

methanol and stirred for 5 h to obtain PFN-Br solution. PTB7-Th:IEICO-4F (1:2 weight ratio, polymer concentration of 24 mg mL^{-1}) was dissolved in CF and stirred for 2 h to obtain polymer solution, and then 1-chloralin was added to the solution at a volume ratio of 0.05% before the experiment.

Device Fabrication: First, an ITO single-sided conductive glass was sequentially sonicated in the water containing detergent, deionized water, ethanol, and acetone for 30 min and then treated with ultraviolet ozone (UV ozone) for 15 min. C_{60} solution was spin-coated on the ITO substrate at 1500 rpm for 60 s. The solution of electrochromic material P3HT was spin-coated on C_{60} at 1500 rpm for 40 s, and then treated by a solvent annealing for 2.5 h and a controlled temperature annealing at 150 °C for 10 min. For tandem solar cells (TSCs), SnO_2 was spin-coated on the ITO conductive glass at 3000 rpm for 30 s and then annealed at 150 °C for 30 min to obtain the electron transport layer. The $CsPbI_2Br$ precursor solution was spin-coated in a nitrogen environment at 500 rpm for 5 s and 3000 rpm for 30 s, respectively, and then annealed at 42 °C and 160 °C for 1.5 min and 10 min, respectively. Then, the P3HT, PBDB-T and PTB7-Th solution was spin-coated at 3000 rpm for 30 s and annealed at 100 °C for 10 min. MoO_3 (8 nm) and Ag (1 nm) were sequentially deposited in a vacuum evaporator at a pressure of 1×10^{-5} Pa. PFN-Br solution was spin-coated at 3000 rpm for 30 s. PTB7-Th:IEICO-4F solution was spin cast onto PFN-Br at 3000 rpm for 60 s. MoO_3 (10 nm) and Ag (100 nm) were sequentially deposited in a vacuum evaporator at a pressure of 1×10^{-5} Pa to obtain the TSCs. Finally, the gel electrolyte was uniformly coated on the surface of the P3HT film, which was also used to firmly stick two ITO/glasses together and complete the I-PVCD.

Material and Device Characterization and Measurement: Current density–voltage (*J–V*) curves of TSCs were measured using by an AAA-grade solar simulator (San-Ei electric Co., Ltd., AM1.5G solar irradiation with a light intensity of 100 mW cm^{-2}) equipped with a Keithley 2400 digital source. A standard Si solar cell purchased from the National Renewable Energy Laboratory was used to calibrate light intensity. The device parameters given in this paper were averaged over 12 individual devices. UV–vis NIR3600 spectrometer (Shimadzu, Japan) was used to measure the absorption and transmittance spectra. External quantum efficiency (EQE) was measured by a QE-R system (Enli Tech., Kaohsiung, Taiwan). In addition, the EQE spectra of front and rear sub-cells were characterized by additionally applying monochromatic light sources (the emission peaks are 850 nm and 500 nm). Ultraviolet photoemission spectroscopy (UPS) was obtained by the Thermo ESCALAB 250XI ultraviolet photoelectron spectrometer equipped with a monochrome ultraviolet light source ($h\nu$ = 21.22 eV). Cyclic voltammetry and electrochemical impedance spectroscopy were performed on an electrochemical workstation (ModuLab XM ECS) using a standard three-electrode system (Tianjin Aida Hengsheng Technology Development Co., Ltd.).

Supporting Information

Supporting Information is available from the Wiley Online Library or from the author.

Acknowledgements

This work was supported by the National Natural Science Foundation of China (52272149 and 62375085); the Natural Science Foundation of Beijing (4212055 and 2222076), the Open Fund of State Key Laboratory of Information Photonics and Optical Communications (IPOC2020A00, Beijing University of Posts and Telecommunications), Beijing Science and Technology Project (Z211100004621010), and 2022 Strategic Research Key Project of Science and Technology Commission of the Ministry of Education, Huaneng Group Headquarters Science and Technology Project (HNKJ20-H88).

Conflict of Interest

The authors declare no conflict of interest.

Data Availability Statement

The data that support the findings of this study are available from the corresponding author upon reasonable request.

Keywords

coloration efficiency, photovoltachromic device, poly(3-hexylthiophene), tandem solar cells, threshold voltage

Received: April 11, 2024
Revised: May 23, 2024
Published online: June 25, 2024

[1] D. M. Kammen, D. A. Sunter, *Science* **2016**, *352*, 922.
[2] N. C. Davy, M. S. Edmonds, J. Gao, X. Lin, A. Liu, N. Yao, A. Kahn, Y. L. Loo, *Nat. Energy* **2017**, *2*, 17104.
[3] J. Li, L. Zhang, J. Cui, X. Lv, M. Feng, M. Ouyang, Z. Chen, D. S. Wright, C. Zhang, *Small* **2023**, *19*, 2303359.
[4] Y. Wang, E. L. Runnerstrom, D. J. Milliron, *Annu. Rev. Chem. Biomol. Eng.* **2016**, *7*, 283.
[5] Y. Bai, C. Zhao, X. Chen, S. Zhang, S. Zhang, T. Hayat, A. Alsaedi, Z. Tan, J. Hou, Y. Li, *J. Mater. Chem. A* **2019**, *7*, 15887.
[6] H. Ling, J. Wu, F. Su, Y. Tian, Y. Liu, *Nat. Commun.* **2021**, *12*, 1010.
[7] J. Wu, M. D. Hsieh, W. Liao, W. Wu, J. Chen, *ACS Nano* **2009**, *3*, 2297.
[8] Y. Liu, J. Wang, F. Wang, Z. Cheng, Y. Fang, Q. Chang, J. Zhu, L. Wang, J. Wang, W. Huang, T. Qin, *Nat. Commun.* **2021**, *12*, 3360.
[9] H. Li, W. Zhang, A. Y. Elezzabi, *Adv. Mater.* **2020**, *32*, 2003574.
[10] A. L. Dyer, R. H. Bulloch, Y. Zhou, B. Kippelen, J. R. Reynolds, F. Zhang, *Adv. Mater.* **2014**, *26*, 4895.
[11] A. Cannavale, G. E. Eperon, P. Cossari, A. Abate, H. J. Snaith, G. Gigli, *Energy Environ. Sci.* **2015**, *8*, 1578.

[12] H. C. Moon, T. P. Lodge, C. D. Frisbie, *Chem. Mater.* **2015**, *27*, 1420.
[13] L. Hsiao, F. Kuo, C. Wu, Y. Huang, Y. Wang, R. Jeng, K. Ho, *Chem. Eng. J.* **2021**, *420*, 129821.
[14] T. Fu, C. Zhao, Y. Zhu, P. Zhang, Y. He, H. Meng, *Org. Electron.* **2021**, *95*, 106189.
[15] K. Xian, Y. Liu, J. Liu, J. Yu, Y. Xing, Z. Peng, K. Zhou, M. Gao, W. Zhao, G. Lu, J. Zhang, J. Hou, Y. Geng, L. Ye, *J. Mater. Chem. A* **2022**, *10*, 3418.
[16] S. Y. Shin, G. Jeong, N. A. M. M. Phu, H. Cheon, V. V. Tran, H. Yoon, M. Chang, *Chem. Mater.* **2023**, *35*, 7460.
[17] J. Huang, C. Yang, C. Hsu, C. Chen, L. Lin, R. Wang, K. Ho, C. Chu, *ACS Appl. Mater. Interfaces* **2009**, *1*, 2821.
[18] Y. Zhao, X. Zhang, W. Li, Z. Li, H. Zhang, M. Chen, W. Sun, Y. Xiao, J. Zhao, Y. Li, *Sol. Energy Mater. Sol. Cells* **2022**, *237*, 111564.
[19] A. Arash, S. A. Tawfik, M. J. S. Spencer, S. K. Jain, S. Arash, A. Mazumder, E. Mayes, F. Rahman, M. Singh, V. Bansal, S. Sriram, S. Walia, M. Bhaskaran, S. Balendhran, *ACS Appl. Mater. Interfaces* **2020**, *12*, 16997.
[20] W. Dong, Y. Lv, L. Xiao, Y. Fan, N. Zhang, X. Liu, *ACS Appl. Mater. Interfaces* **2016**, *8*, 33842.
[21] S. Li, Y. Wang, J. Wu, L. Guo, M. Ye, Y. Shao, R. Wang, C. Zhao, A. Wei, *RSC Adv.* **2016**, *6*, 72037.
[22] A. Chaudhary, D. K. Pathak, S. Mishra S, P. Yogi, P. R. Sagdeo, R. Kumar, *Phys. Status Solidi A* **2019**, *216*, 1800680.
[23] P. Shi, J. Wang, Z. Guo, *Chem. Eng. J.* **2023**, *451*, 139082.
[24] S. Zhang, P. Lei, J. Fu, X. Tong, Z. Wang, G. Cai, *Appl. Surf. Sci.* **2023**, *607*, 155015.
[25] A. Chaudhary, D. K. Pathak, M. Tanwar, P. Yogi, P. R. Sagdeo, R. Kumar, *ACS Appl. Electron. Mater.* **2019**, *1*, 58.
[26] X. Lv, J. Li, L. Zhang, M. Ouyang, A. Tameev, A. Nekrasov, G. Kim, C. Zhang, *Chem. Eng. J.* **2022**, *431*, 133733.
[27] M. Shao, D. Ji, Z. Xu, J. Dong, X. Lv, M. Ouyang, Y. Lv, D. S. Wright, C. Zhang, *J. Power Sources* **2023**, *581*, 233490.
[28] T. H. Kim, S. H. Song, H. J. Kim, S. H. Oh, S. Han, G. Kim, Y. C. Nah, *Appl. Surf. Sci.* **2018**, *442*, 78.
[29] G. Yang, Y. M. Zhang, Y. Cai, B. Yang, C. Gu, S. X. A. Zhang, *Chem. Soc. Rev.* **2020**, *49*, 8687.
[30] T. Yu, P. Theato, H. Yao, H. Liu, Y. Di, Z. Sun, S. Guan, *Chem. Eng. J.* **2023**, *451*, 138441.
[31] H. Meng, in *Organic Electronics for Electrochromic Materials and Devices*, John Wiley & Sons, New York, NY, USA **2021**.
[32] *International organization for standardization. -ISO 9050:2003(en) glass in building*. https://www.iso.org/obp/ui/#iso:std:iso:9050:ed-2:v1:en.
[33] B. Yedikardeş, M. Altun, E. Zayim, *Synth. Met.* **2023**, *297*, 117407.
[34] X. Xia, Z. Ku, D. Zhou, Y. Zhong, Y. Zhang, Y. Wang, M. Huang, J. Tu, H. Fan, *Mater. Horiz.* **2016**, *3*, 588.
[35] Y. Zhang, L. Kong, Y. Zhang, H. Du, J. Zhao, S. Chen, Y. Xie, Y. Wang, *Org. Electron.* **2020**, *81*, 105685.
[36] J. Bertrandie, J. Han, C. S. P. D. Castro, E. Yengel, J. Gorenflot, T. Anthopoulos, F. Laquai, A. Sharma, D. Baran, *Adv. Mater.* **2022**, *34*, 2202575.
[37] P. M. Beaujuge, S. V. Vasilyeva, D. Y. Liu, S. Ellinger, T. D. McCarley, J. R. Reynolds, *Chem. Mater.* **2012**, *24*, 255.
[38] R. Zeng, L. Zhu, M. Zhang, W. Zhong, G. Zhou, J. Zhuang, T. Hao, Z. Zhou, L. Zhou, N. Hartmann, X. Xue, H. Jing, F. Han, Y. Bai, H. Wu, Z. Tang, Y. Zou, H. Zhu, C. C. Chen, Y. Zhang, F. Liu, *Nat. Commun.* **2023**, *14*, 4148.
[39] Y. E. Firat, A. Peksoz, *Electrochim. Acta* **2019**, *295*, 645.
[40] R. Gonçalves, E. C. Pereira, L. F. Marchesi, *Int. J. Electrochem. Sci.* **2017**, *12*, 1983.
[41] W. Schuhmann, C. Kranz, H. Wohlschläger, J. Strohmeier, *Biosens. Bioelectron.* **1997**, *12*, 1157.
[42] F. R. Simões, L. A. Pocrifka, L. F. Q. P. Marchesi, E. C. Pereira, *J. Phys. Chem. B* **2011**, *115*, 11092.
[43] L. Hostert, G. Alvarenga, M. Vidotti, L. F. Marchesi, *J. Electroanal. Chem.* **2016**, *774*, 31.
[44] Y. Kim, Y. Kim, S. Kim, E. Kim, *ACS Nano* **2010**, *4*, 5277.
[45] P. S. Patil, S. H. Mujawar, A. I. Inamdar, S. B. Sadale, *Appl. Surf. Sci.* **2005**, *250*, 117.
[46] W. Shen, Y. Dong, F. Huang, Y.-B. Cheng, J. Zhong, *Mater. Rep. Energy* **2021**, *1*, 100060.
[47] Z. He, H. Xu, Y. Zhang, Y. Hou, H. Niu, *Polymers* **2022**, *14*, 4965.
[48] Y. Bai, F. Han, R. Zeng, S. Tian, F. Wang, X. Wang, M. Dai, M. Li, Z. Tan, *J. Mater. Chem. A* **2023**, *11*, 17514.
[49] Q. Fu, H. Liu, S. Li, T. Zhou, M. Chen, Y. Yang, J. Wang, R. Wang, Y. Chen, Y. Liu, *Angew. Chem.* **2022**, *134*, 202210356.
[50] X. Wang, Z. He, H. Chen, L. Yao, C. Li, X. Lin, Z. Zhou, K. Li, W. Wang, W. Cai, Q. Ling, H. Zhen, *Adv. Funct. Mater.* **2023**, *33*, 2308435.
[51] Y. Cai, Q. Li, G. Lu, H. S. Ryu, Y. Li, H. Jin, Z. Chen, Z. Tang, G. Lu, X. Hao, H. Y. Woo, C. Zhang, Y. Sun, *Nat. Commun.* **2022**, *13*, 2369.
[52] Y. Bai, C. Zhao, S. Zhang, S. Zhang, R. Yu, J. Hou, Z. Tan, Y. Li, *Sci. China Chem.* **2020**, *63*, 957.